Effect of stereochemistry on nanoscale assembly of ABA triblock copolymers with crystallizable blocks

Xuechen Yin,[a] David R.O. Hewitt,[a] Bingqian Zheng,[a] Suan P. Quah,[a] Christopher B. Stanley,[b] Robert B. Grubbs,[a] and Surita R. Bhatia*

[a]*Department of Chemistry, Stony Brook University, Stony Brook, NY 11794*

[b]*Computational Sciences and Engineering Division, Oak Ridge National Laboratory, Oak Ridge, TN 37831*

*Corresponding author: Surita.bhatia@stonybrook.edu

1. Abstract

We report on the nanoscale assembly of poly(lactic acid)-*b*-poly(ethylene oxide)-*b*-poly(lactic acid) (PLA-PEO-PLA) triblock copolymers in water, focusing on the effect of stereochemistry, where the PLA blocks are statistical copolymers of L-lactide and D-lactide with L/D ratios of 100/0, 95/5, 90/10, 85/15, 75/25, and 50/50. Small-angle neutron scattering (SANS) shows a nearly constant *d*-spacing as concentration varies in triblock systems with L/D ratios of 90/10 and 95/5, which we attribute to inhomogeneity in the structure of these gels, supported by previous USANS and confocal microscopy studies. The SANS data fit well to a core-shell ellipsoid form factor model with a hard-sphere structure factor. Polymeric micelles with L/D ratios from 75/25 to 85/15 displayed very high aggregation numbers, consistent with a strong interaction between PLA chains and the enhanced storage modulus observed in rheological studies of these systems. While the 90/10 and 95/5 samples showed lower aggregation numbers, their SANS profiles shows close spacing between micelles, which may promote a high fraction of intermicellar bridging chains, also consistent with a higher storage modulus. Overall, these results provide insight into the micellar assembly behavior of block copolymers with a crystallizable block, and indicate that tuning stereochemistry of PLA-based block copolymers is an effective means of modifying micellar properties for specific applications.

2. Introduction

Biocompatible polymers, including amphiphilic block copolymers, have been explored for applications in delivery, biomedical devices, and replacement of soft tissues [1-3]. Amphiphilic block copolymers self-assemble in aqueous media due to the relative hydrophobicity of selective blocks, and various structures such as spheres, ellipsoids, cylinders, and lamellae can be formed

[4,5]. Transport properties and rheology are often strongly dependent upon the nanoscale structure in these systems. Because the types of monomers used for these applications are constrained by requirements for biocompatibility, new strategies are needed to generate the range of self-assembled structures needed to optimize the properties needed for end applications in drug delivery and biomedical devices [6-11].

Poly(lactide)-*block*-poly(ethylene oxide)-*block*-poly(lactide) (PLA-PEO-PLA), an ABA amphiphilic triblock copolymer, has been widely studied for biomedical applications, due to the biocompatible nature of both blocks and the biodegradability characteristics of the PLA blocks, as well as the ability to tune the assembly, release characteristics, and rheology of the system [12-14]. A range of self-assembled structures has been observed in these systems both through experiments and theory. Self-assembly in PLA-PEO-PLA copolymers has been studied by controlling the PLA endblock length, incorporating nanoparticles, and adjusting the physical crosslinks from amorphous to crystalline.[15-17] For example, Kimura and coworkers reported thermo-sensitive hydrogels mixtures of enantiomeric PLLA-PEG-PLLA and PDLA-PEG-PDLA triblock copolymers with sol-gel transition around 37 °C. The mechanism of gelation was proposed to be the interaction of micelles including stereocomplex formation between PLLA and PDLA blocks as well as the exchange of PLA blocks in the micellar cores. [18] Dissipative particle dynamics (DPD) were utilized by Pricl to simulate the self-assembly of racemic PLA and PEO copolymers with AB diblock and ABA triblock architectures in aqueous media, and morphological phase diagrams were obtained for both the copolymers alone as well as for the copolymers in the presence of model hydrophobic drugs with different drug loading levels [19]. DPD simulations by Zhou and coworkers on diblock copolymers show the presence of dumbbell-like assemblies; [20] however, this may be an artifact of edge effects due to the small

volume used in these simulations, and the hydrophilic blocks in their simulations appear to have an extra methylene group and would be significantly more hydrophobic than PEG. In experimental small-angle neutron scattering (SANS) studies, Nystrom et al. demonstrated a transition from an asymmetric ellipsoid structure to a spherical core-shell structure in a PLGA-PEG-PLGA system with increasing PEG-spacer in the dilute regime[5]. O'Reilly and Dove have reported the reorganization of cylindrical micelles to spherical micelles driven by stereocomplexation in mixed PEO-b-PLLA/ PEO-b-PDLA solutions [21]. The morphological transition was further confirmed by fitting results obtained from *in situ* synchrotron small-angle X-ray scattering (SAXS). More recently, the same authors have demonstrated solvent- and composition-tunable 1D and 2D nanostructures in poly(lactide)-containing block copolymers [22,23].

Poly(L-lactic acid) (PLLA), poly(D, L-lactic acid) (PDLLA), and the mixture with both PLLA and PDLA are typical forms researchers have worked on to study the effect of PLA stereochemistry on material performance and microscopic structure in PLA-containing block copolymer [17,24,25]. The formation of stereocomplexes and the interaction between PDLA and PLLA has been reported experimentally to significantly enhance mechanical properties and thermal stability. [26] However, the impact of stereochemistry with L/D ratios between 50/50 and 100/0 in PLA block on the nanostructure is still not well-understood. More quantitative characterization and modeling of polymer structure in the solution and gel state is necessary to promote the shrinking of the gap between polymer design and application. In collaborative work with Tew, we have previously demonstrated the self-assembly of associative PLLA-PEO-PLLA hydrogels into disk-like nanostructures with crystalline PLLA domains, in contrast to PRLA-PEO-PRLA hydrogels, which form spherical structures with amorphous PRLA cores [4,27].

Furthermore, at the microscale these systems have been shown to have a mass fractal structure with water channels among a polydisperse network of microaggregates [28], and drug release behavior of these gels was shown to be dependent upon the stereochemistry [29]. More recently, we have reported the rheological behavior and microscale structure of PLA-PEO-PLA triblock copolymers with varied stereochemistry of PLA blocks from L/D ratios of 50/50 to 100/0. A non-monotonic dependence of *G'*, maximum in *G'*, and decreased intermicellar spacing at intermediate L/D ratios were found [30], with a range of large-scale microstructures seen in ultra-small angle neutron scattering (USANS) and confocal microscopy. [31] We expect the rheological properties and self-assembly behavior of this series of copolymers to be similar to that of copolymers with stereochemistry of PLA blocks from L/D ratios of 0/100 to 50/50. Developing a more in-depth understanding to the self-assembly of these stereochemically varied triblock copolymers is crucial to optimizing design and performance of these materials in biomedical devices.

3. Materials and Methods

3.1 Materials and triblock copolymer synthesis

L-Lactide and D,L-lactide (a racemic mixture of D-lactide and L-lactide) from Acros Organics and Sigma Aldrich were both recrystallized from either ethyl acetate or toluene and stored in a nitrogen-filled glove box. Polyethylene oxide (PEO-10k, M_n = 10 kg/mol, Alfa Aesar) was freeze-dried or vacuum dried at 40 °C for two days and stored in a nitrogen-filled glove box [32]. 1,8-Diazabicyclo[5.4.0]undec-7-ene (DBU) was obtained from Santa Cruz Biotechnology and used without additional purification. All aqueous solutions were prepared in water purified with a Barnstead Nanopure system (resistivity = 18 MΩ-cm).

The detailed synthesis method is based on previously reported approaches [18,33-35]. In a nitrogen-filled glove box, PEO-10k (1.2 g, 0.12 mmol) was loaded into a round-bottom flask equipped with a magnetic stir bar, sealed with a rubber septum, and removed from the glove box. In the same glove box, D,L-lactide (0.62 g, 4.3 mmol) was loaded into a scintillation vial, removed from the glove box, and dichloromethane (12 mL) was added to the vial via a nitrogen-purged syringe. The vial was swirled to ensure complete dissolution with the syringe still inserted. Using the same syringe, the lactide solution in dichloromethane was subsequently added to the round-bottom flask containing the PEO-10k. A solution of DBU (0.04 g, 0.26 mmol) in dichloromethane (4.0 mL) was prepared in the glove box and transferred by syringe to the round-bottom flask containing the PEO-10k/lactide solution. The reaction was stirred under nitrogen for 4 h at room temperature, then concentrated with a rotary evaporator. The crude polymer was then precipitated by addition of the concentrated solution into hexanes (70 mL). The supernatant was decanted, and the solid polymer was dried in a vacuum oven at 40 °C for 3 days. Typical yields were >80%, with monomer conversions >95% determined by ^{1}H NMR (400 MHz, $CDCl_3$), by comparison of polymer methine protons to residual monomer methine protons. ^{1}H NMR of isolated PLA-PEO-PLA (400 MHz, $CDCl_3$): δ 5.17 (m, –OOC–C<u>H</u>(CH_3)–), 4.32 (m, –OOC–C<u>H</u>(CH_3)–OH), 4.21 (m, COO–C<u>H_2</u>– C<u>H_2</u>–OPEO), 3.56 (m, –CH_2–CH_2–O–), 1.57 (d, –OOC–CH(C<u>H</u>$_3$)–) ppm. (Figure S1-2). Characteristics of polymers synthesized are provided in Table 1.

Table 1. The characteristics of PLA-PEO-PLA triblock copolymers synthesized.

Sample	$Đ$[a]	RU_{PLA}[b]	M_n (Da)	L/D ratio

S 50/50	1.21	88	16,338	50/50
S 75/25	1.16	75	15,402	75/25
S 80/20	1.21	82	15,960	80/20
S 85/15	1.10	77	15,546	85/15
S 90/10	1.22	81	15,834	90/10
S 95/5	1.17	85	16,122	95/5
S 100/0	1.26	82	15,960	100/0

[a]Dispersity, *Đ*, determined by size-exclusion chromatography in THF with polystyrene standards. [b]Total lactide repeat units (RU_{PLA}) determined by ^{1}H NMR spectroscopy.

3.2 Preparation of polymer solutions and gels

Each gel was prepared by the slow addition of dried PLA-PEO-PLA powder to a fixed mass of deuterated water (D_2O), over a period of about two hours, followed by stirring with a magnetic stir bar. When the viscosity of solution increased to the point where magnetic stirring was no longer effective, manual stirring with a spatula was employed until the polymer was completely added and the mixtures appeared homogeneous. The solutions were allowed to equilibrate for at least one day at room temperature in sealed vials to ensure full dissolution of polymers in D_2O. The concentration of gel samples used for SANS was initially 10 wt%. Further dilution of gel samples with D_2O after each scattering test generated additional gels and solutions with polymer concentrations of 8 wt%, 5 wt%, and 2 wt%.

3.3 SANS characterization

SANS measurements were conducted on the Extended Q-range Small-angle Neutron Scattering diffractometer (beamline 6, EQ-SANS) at the Spallation Neutron Source (SNS) located at Oak Ridge National Laboratory (ORNL), Oak Ridge, TN. Samples were placed in 1 mm quartz banjo cells, placed in an aluminum cell holder. Spectra were obtained at 25°C for all the samples. The q range covered in experiments was 0.002 $Å^{-1} < q < 1$ $Å^{-1}$. The low-angle detector can travel along the beam, giving a variable sample to detector distance of 1.3 to 9 m. Data reduction and normalization were performed using standard techniques within MantidPlot [36], and all SANS data reported here are on an absolute scale [37] except where noted. Scattering length densities (SLD) used in data fitting and calculation are 1.73×10^{-6}, 6.38×10^{-7}, and 6.36×10^{-6} $Å^{-2}$ for PLA, PEO and D_2O, respectively. [4]

4. Results and Discussion

4.1 Model Independent Analysis of Scattering Data

SANS experiments were conducted at concentrations of 2 wt%, 5 wt%, 8 wt%, and 10 wt%. We expect these amphiphilic ABA triblock copolymers to form associated micelles, sometimes referred to as "flowerlike micelles" [38-41], in aqueous media. Representative curves for the 50/50, 85/15, and 90/10 systems are shown in Figure 1; data for all polymers is in the SI. SANS data has been processed with background subtraction. The 85/15, 90/10, and 95/5 copolymers each showed a broad peak at all measured concentrations. However, copolymers with other L/D ratios such as 50/50 and 100/0 only showed a weak correlation peak at 10 wt%, and a shoulder at lower concentrations. A shoulder is characterized by the slower decay without a maximum in scattering intensity, while a peak is observed when the interaction of neighboring micelles is stronger and the structures tend to be more ordered. A clear local maximum of

scattering intensity can be found at a particular q value in this case. For these samples, we expect that the intermicellar interactions are not strong enough to have a significant effect on the structure factor at lower concentrations. This suggests that the strongest intermicellar interactions are present for copolymers with intermediate L/D ratios, which is consistent with our previous rheological studies that showed a maximum in the storage modulus at intermediate L/D ratios.[30]

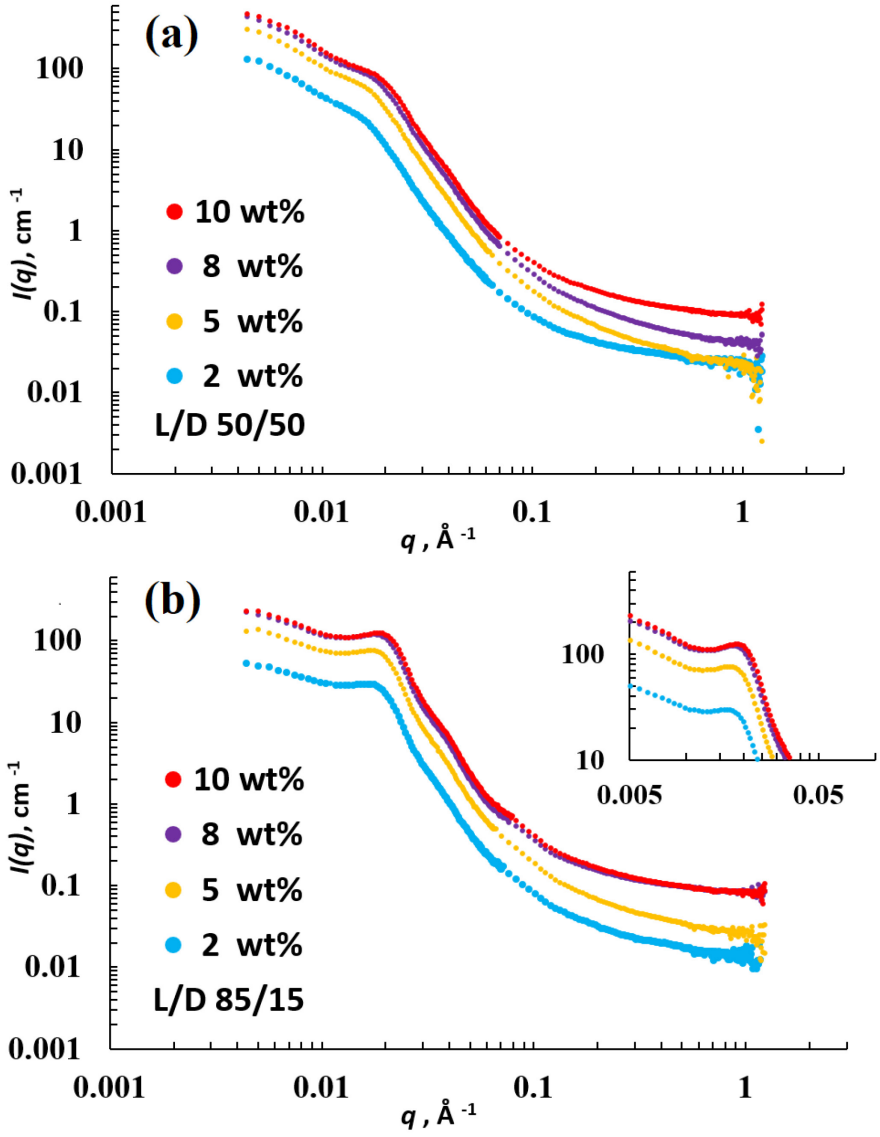

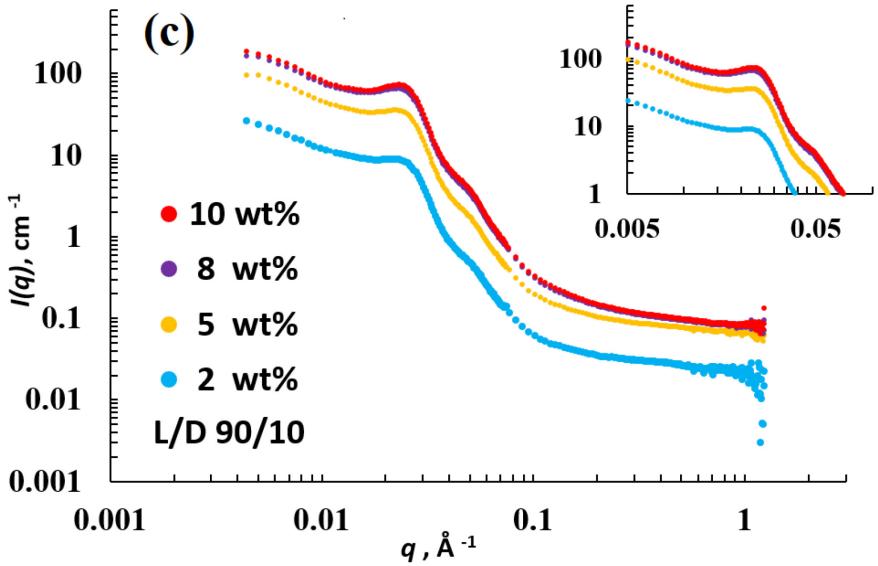

Figure 1. Representative SANS spectra of PLA-PEO-PLA triblock copolymer gels and solutions with (a) L/D 50/50, (b) L/D 85/15, and (c) L/D 90/10 at different concentrations. Inset: Magnified section of the area around the correlation peaks.

SANS spectra for the L/D 85/15 copolymer are shown in Figure 1b. For this sample, increasing the concentration leads to a shift of correlation peak to higher wave vector *q*. This indicates a decrease in the intermicellar spacing, or *d*-spacing, as concentration increases (Figure 2). This is a typical result for micellar gels [4]. By contrast, the 90/10 sample does not show a change in the *d*-spacing as concentration increases (Figure 1c, Figure 2); and similar behavior is seen for the 95/5 system (Supplementary Information, Figure S3c). This could be due to inhomogeneity in the structure of the 90/10 and 95/5 gels, where larger structures comprising several micelles form upon initial dispersion, and interactions between micelles are sufficiently strong that the clusters persist at lower concentration (Figure 3). Our previous USANS and confocal microscopy studies [31] show evidence of microscale inhomogeneities in these gels that are several hundred times larger than an individual micelle, consistent with this idea.

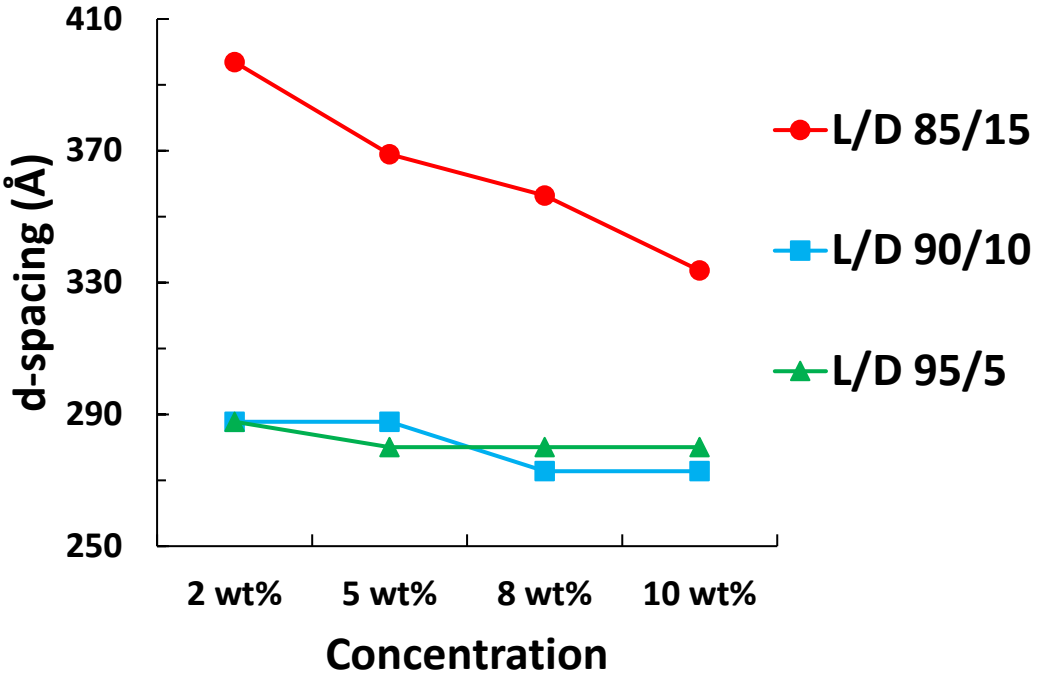

Figure 2. Change in *d*-spacing of copolymer gels or solutions with L/D ratios 85/15, 90/10, and 95/5 at increasing concentration.

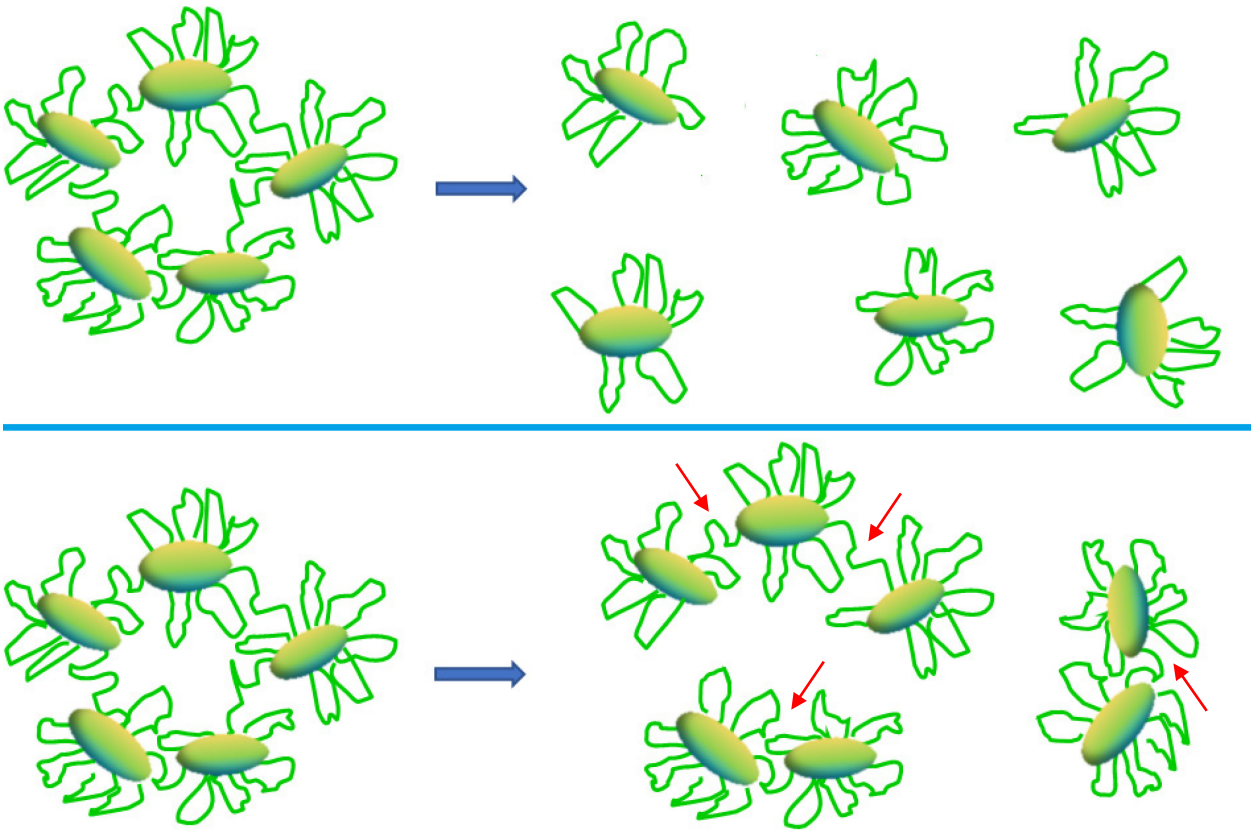

Figure 3. Possible structures consistent with change in *d*-spacing upon dilution for different

micellar gels. Top: Micelles homogeneously distribute themselves further apart at lower concentrations, leading to the expected increase in *d*-spacing at lower concentration, as observed in the 85/15 gels. Bottom: Strong intermicellar attractions (red arrows) lead to persistent clusters at lower concentrations, and *d*-spacing does not change with concentration, as is seen in the 90/10 and 95/5 gels.

4.2 Kratky Analysis

The scattered intensity can be written in terms of models for the form factor P(q), the structure factor S(q), and other experimental parameters, including the number density of scattering centers and scattering length density (SLD) contrast between particles and solvent. The form factor, indicative of particle shape, can more cleanly be obtained from experiments performed at low concentrations, where S(q) is expected to be 1. By contrast, S(q), which arises from interparticle correlations between the scattering centers, plays an increasingly important role at higher concentrations.

A spherical core-shell form factor model and a disk-like form factor model have previously been utilized to fit the scattering spectra of PRLA-PEO-PRLA and PLLA-PEO-PLLA copolymer systems, respectively [4]. Additionally, a hard sphere structure factor was introduced to account for repulsive interactions. Although the core-shell sphere and disk-like micelle models provided reasonably good fits to the data for samples with L/D ratios of 50/50 and 100/0, [4] respectively; the PLA chains in the present study have intermediate L/D ratios, and our previous XRD measurements indicate that the PLA micelle cores are not fully crystalline for these systems. [30] Thus, we explored utilizing other types of form factor models and micellar shapes to describe these micelles.

In order to select the appropriate model to fit the PLA-PEO-PLA systems with different L/D ratios, Kratky plots were prepared. Kratky plots, obtained by plotting I(q)*q^2 versus q,

minimize the low-q features in scattering and highlight the high-q behavior of the scattered intensity. For biological macromolecules, Kratky plots have been widely used to qualitatively assess the extent of random-coil nature present in the macromolecular conformation and to distinguish folded states from unfolded states, due to the Kratky analysis's sensitivity to the morphology and compactness of scattering objects. [42] For polymer systems, analysis of Kratky plots also provides insight into structure. For instance, a Kratky plot representation of the scattered intensity from Gaussian chains is expected to initially show a monotonic increase and then approach a plateau at high q. A slight change in slope before the plateau region can result from different types of chain architecture such as stars, rings, and branched chains [43]. To gain insight into the micellar structure and shape, the SANS data for PLA-PEO-PLA gels were replotted on Kratky plots. Representative data are shown in Figure 4, and data for other copolymers are included in the Supplementary Information (Figure S4). Peaks at low q are found for the entire series of copolymer gels at all concentrations measured.

The high q region of Kratky plot generally receives less attention compared to that at low-q and mid-q. However, the interpretation of results at high q can still provide insight into structural changes. It is noticeable that the Kratky plot at mid-q shows a minimum, and then subsequently a nonlinear increase at high q without any plateau. Perahia and coworkers, who observed similar behavior in assemblies of a sulfonated pentablock system, attributed this behavior to a divergence from sphericity in the assemblies, and applied a core-shell ellipsoid model to fit their scattering data [44].

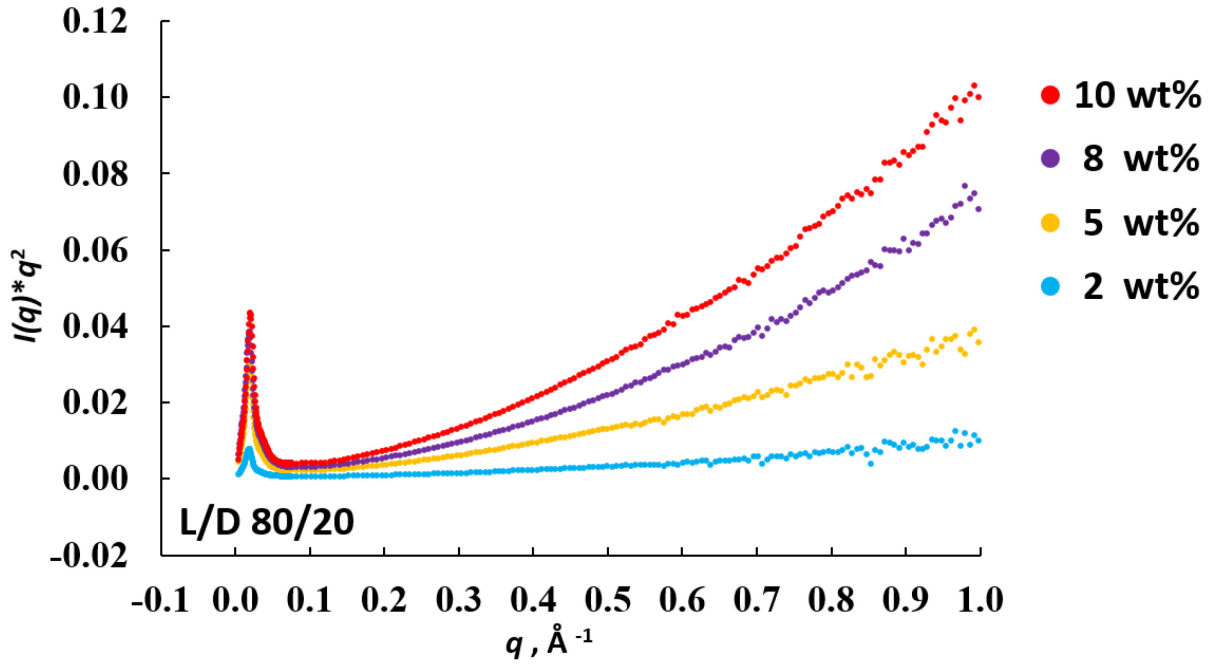

Figure 4. Representative Kratky plot of PLA triblocks with L/D 80/20 at different concentrations.

4.3 Core-shell Model Fits to Scattering Data

Motivated by our Kratky analysis, we chose to use a core-shell ellipsoid model to perform detailed fits of our SANS data. The diagram describing the geometric parameters in core-shell ellipsoid model is shown in Figure 5. The equatorial radius of the core and thickness of the shell at equator are given by R_{equat} and d_{equat}, respectively. Likewise, R_{polar} is the radius of the core at the pole, while d_{polar} indicates the polar thickness of shell. The overall radii of the core and shell together in the equatorial and polar directions are then $R_{tot,eq} = R_{equat} + d_{equat}$ and $R_{tot,pol} = R_{polar} + d_{polar,}$ respectively. The axial ratio of the core X_{core}, given as R_{polar} / R_{equat}, can further describe the circular symmetry in the ellipsoid. For the PLA-PEO-PLA micelles in this study, X_{core} values were found to be > 1, indicating that the micellar core is a prolate ellipsoid, rather than an oblate ellipsoid ($X_{core} < 1$) or a sphere ($X_{core} = 1$) [45,46]. With this model, the scattered intensity arising from the form factor is given by:

$$P(q) = \frac{\text{scale}}{V} F^2(q, \alpha) + \text{background} \quad (1)$$

With:

$$\mathrm{F}(q,\alpha) = \mathrm{p}\left(q, R_{equat}, R_{polar}, \alpha\right) + \mathrm{p}\left(q, R_{tot,eq}, R_{tot,pol}, \alpha\right) \quad (2)$$

$$\mathrm{p}\left(q, R_{equat}, R_{polar}, \alpha\right) = 3\Delta\rho V \frac{\{\sin[\,q\mathrm{m}(R_{equat},R_{polar},\alpha)\,] - \cos[\,q\mathrm{m}(R_{equat},R_{polar},\alpha)\,]\}}{[q\mathrm{m}(R_{equat},R_{polar},\alpha)]^3} \quad (3)$$

$$\mathrm{m}(R_{equat}, R_{polar}, \alpha) = (R_{equat}^2 \sin^2\alpha + R_{polar}^2 \cos^2\alpha)^{0.5} \quad (4)$$

Here V is the volume of the ellipsoid, $\Delta\rho$ is the scattering length density contrast between the scatterer and the solvent, and α is the angle between the axis of the ellipsoidal structure and scattering vector. We assume the ellipsoids are randomly oriented to obtain:

$$\mathrm{F}^2(q) = \int_0^{\pi/2} \mathrm{F}^2(q,\alpha)\sin(\alpha)\, d\alpha \quad (5)$$

A polydispersity factor, Σ, based on a Schulz distribution function of the equatorial size of micellar core was introduced in the model fitting to effectively describe the micelle sizes. [47]

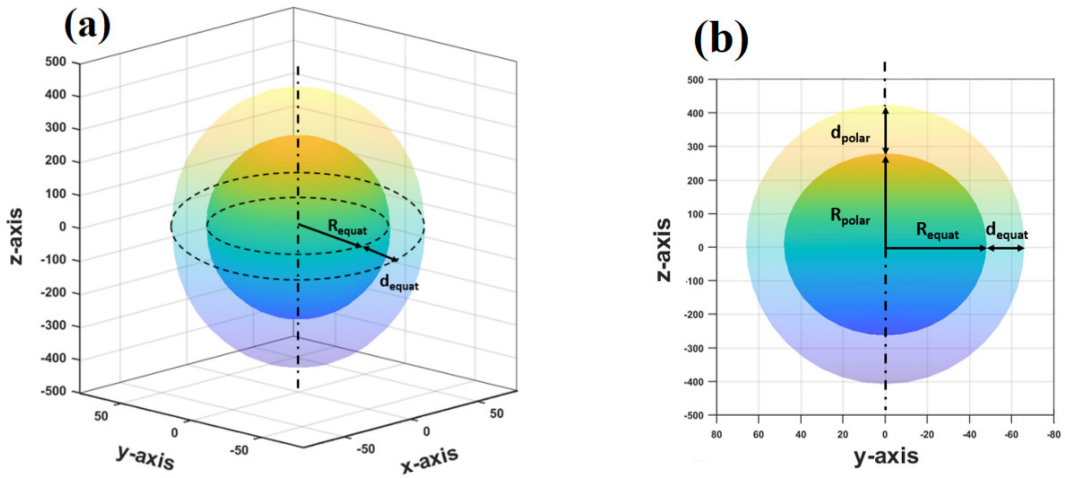

Figure 5. The geometric parameters of core-shell ellipsoid model shown in (a) 3D ellipsoid with circular equator (b) *yz* plane cross section of the prolate ellipsoid.

SANS fits for systems with different L/D ratios at 10 wt% are displayed in Figure 6; fitting results from other concentrations are in the Supplementary Information (Figure S5). The

obvious correlation peaks in the curves for L/D 75/25, 80/20, 85/15, 90/10, and 95/5 systems necessitate the inclusion of a structure factor; we utilized a polydisperse hard-sphere structure factor with Percus-Yevick closure to account for the contribution of interparticle interference to the scattering intensity [48]. This gives an additional fitting parameter, the volume fraction of hard spheres (φ_i) which describes the nonoverlapping region occupied by hard spheres. Although the micelles are not strictly spheres, the polydisperse hard-sphere structure factor is often applied in scattering studies of more complex assemblies, such as SAXS studies of α-crystallin [49] and SANS studies of a variety of block copolymer assemblies [4].

In general, the fits (Figure 6) agree well with the scattering profiles at low q and mid q, while diverging at high q due to the presence of larger-scale aggregates in our system, which we have previously observed via USANS and confocal microscopy [31] but which are not included in the micellar model used here. [50] Because data at $q < 0.01$ are likely to be affected by the presence of large microscale structures, they were not included in the fitting analysis. We have previously analyzed these large structures in more detail with USANS and confocal microscopy [31].

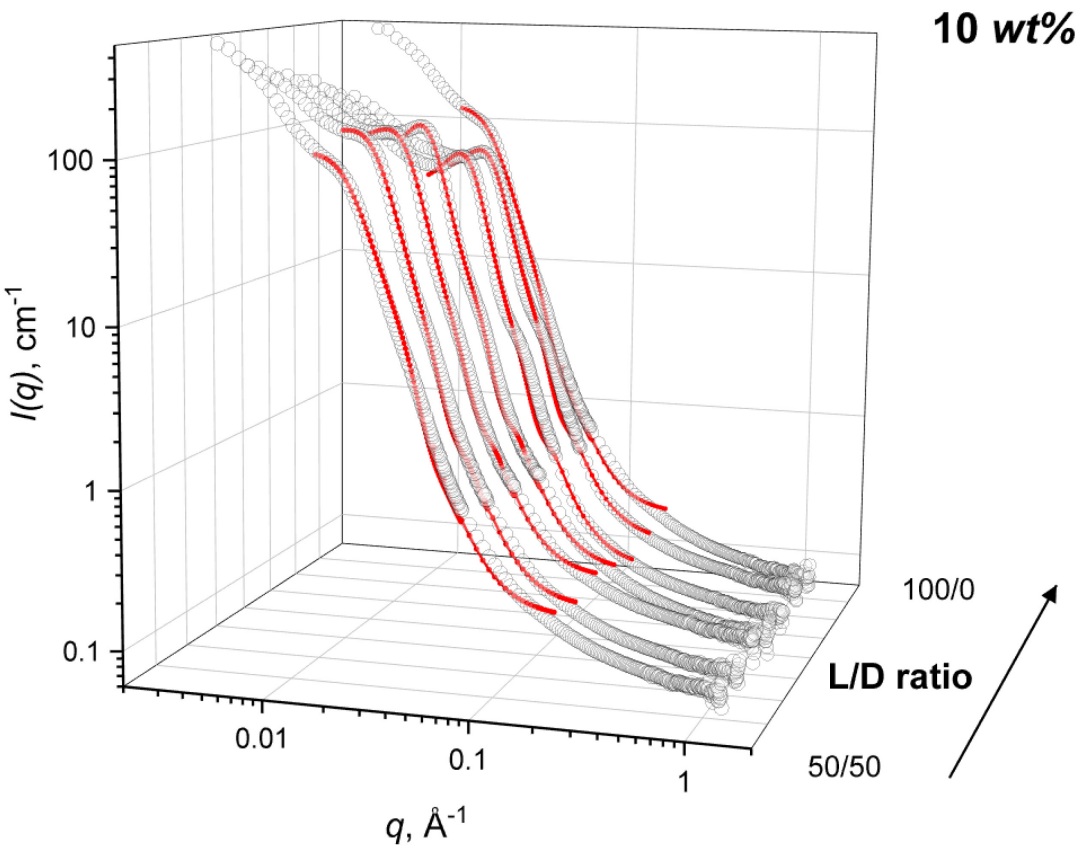

Figure 6. Representative fits of SANS spectra for PLA-PEO-PLA triblock copolymer gels at 10 wt% with different L/D ratio to the core-shell ellipsoid model.

Detailed SANS fitting parameters for PLA-PEO-PLA copolymer systems with different stereochemistry of the PLA blocks at concentrations of 5, 8, and 10 wt% are summarized in Table 2 and Table S1. The parameters describing the micelle shape and size do not depend strongly on concentration for each L/D system. This is consistent with previous studies of PLA-PEO-PLA gels with different PLA lengths than studied here and L/D ratios of 50/50 and 100/0 [4]. For 10 wt% polymer solutions, maximum R_{equat} is observed for triblock copolymers with intermediate L/D ratios (57.6 Å for 75/25 and 57.3 Å for 80/20), while the lowest R_{equat} value (44.2 Å) is found at an L/D ratio of 95/5. PLA-PEO-PLA series with L/D 50/50 and 100/0 at 10 wt% have the R_{equat} in between compared to that for intermediate L/D and higher L/D ratios (90/10 and 95/5). With these

parameters, a core volume can be calculated, allowing us to generate a three-dimensional image of the micelles. For some samples, we believe the crystalline domains in the PLA core region leads to ellipsoids with large X_{core} values; previous studies of similar types of PLA-PEO-PLA copolymers in water have also shown micelles with anisotropic shapes such as disks.[4,27] A visualization of the core-shell ellipsoid micelles, generated using Matlab, is shown in Figure S6.

We previously found a non-monotonic trend in the storage modulus of these gels with L/D ratio,[30] where gels with an intermediate L/D ratio displayed a higher *G'* than the 50/50 or 100/0 gels, and the highest moduli were obtained for L/D ratios in the range of 75/25 to 85/15. We hypothesized that the behavior of *G'* with L/D ratio was due to a competition between an increase in the time for PLA endblocks to pull out of micelles as the L/D ratio is increased and PLLA crystallization occurs, and a decrease in the number of bridging chains for micelles with crystalline PLA domains, as formation of bridges may be hindered by crowded crystalline PLA domains.

Although we cannot directly obtain information about the fraction of bridging chains or the timescale for PLA endblock pull-out from SANS data, we can make some estimates of how these parameters will vary in these series of polymers, based on structural parameters obtained from SANS. Theories of associative polymers suggest that the timescale for endblock pull-out from micelles should be related to the strength of interaction between hydrophobic blocks. A stronger interaction between hydrophobic blocks will likely also lead to larger aggregation numbers. [51] Micelles of the polymers at intermediate L/D ratios of 75/25, 80/20, and 85/15 do indeed have a higher aggregation number than the 50/50, 90/10, 95/5, and 100/0 polymers. Polymers in this range also form gels with the highest storage modulus. Thus, the trend in aggregation number with L/D ratio is consistent with our expectations from rheology.

However, as discussed above, there must be another factor impacting the rheology, as the

the aggregation number and overall micelle size for L/D 90/10 and 95/5 are smaller than the 50/50 and 100/0 samples, while these samples also display a higher storage moduli than the 50/50 and 100/0 systems. [30] We had hypothesized that the fraction of bridging chains would also be an important factor. While we cannot calculate this directly, theories of associative micellar gels suggest a higher fraction of bridging chains when the intermicellar distance is smaller, until the fraction of bridging chains reaches a limiting equilibrium value at close spacings. [52,53] We do in fact find a decreased *d*-spacing (d_{sc}) for intermediate L/D ratios, as estimated from the peak position for the 10 wt% samples [30]. This value of the *d*-spacing is derived from the peak position and thus averages over all orientations of the micelles present in the gels. We can estimate the distance between the edge of the PEO shells of the micelles in the equatorial direction for the 10 wt% samples, which we term $d_{micelle}$, as $d_{micelle} = d_{sc} - 2R_{tot,eq}$. We note that this is only an estimate, but it represents the smallest distance that a bridging chain would need to span between micelles and thus gives insight into the probability that a given system will have more or less bridging chains. The decreased *d*-spacing together with the larger dimension of the micelles in the equatorial direction, $R_{tot,eq}$, at these L/D ratios leads to a smaller distance between the edge of PEO shells in the gels with intermediate L/D ratios as compared to the 50/50 and 100/0 systems (Table 3). Therefore, we may expect formation of more intermicellar bridging chains in gels at intermediate L/D ratios, which contribute to greater elasticity of these associative gels as compared to the 50/50 and 100/0 gels, consistent with our previous hypothesis on the origin of the rheological trends we observed. [30] In addition, we are unable to obtain the distance between PEO shells from the polar direction due to much larger geometric parameters. The PEO shells of neighboring core-shell ellipsoids are physically in contact and interacting along the polar direction in this case.

Table 2. Parameters of micelle in core-shell ellipsoid model of PLA-PEO-PLA systems with different L/D ratios at 10 wt%.

Parameter		L/D 50/50	L/D 75/25	L/D 80/20	L/D 85/15	L/D 90/10	L/D 95/5	L/D 100/0
core	R_{equat} (Å)	48.1 ± 0.2	57.6 ± 0.2	57.3 ± 0.1	53.1 ± 0.1	51.2 ± 0.1	44.2 ± 0.1	50.6 ± 0.1
	X_{core}	5.64 ± 0.05	4.40 ± 0.04	4.02 ± 0.02	4.87 ± 0.04	3.71 ± 0.02	4.68 ± 0.03	5.14 ± 0.04
	R_{polar} (Å)	271.3 ± 3.5	253.4 ± 3.2	230.3 ± 1.6	258.6 ± 2.6	190.0 ± 1.4	206.9 ± 1.8	260.1 ± 2.6
shell	d_{equat} (Å)	18.1 ± 0.2	20.9± 0.2	20.7 ± 0.1	20.7 ± 0.2	12.8 ± 0.1	14.8 ± 0.1	19.8 ± 0.2
	X_{shell}	8.04 ± 0.12	5.19 ± 0.08	5.21 ± 0.06	4.74 ± 0.08	6.09 ± 0.08	4.90 ± 0.09	6.01 ± 0.08
	d_{polar} (Å)	145.5 ± 3.8	108.5 ± 2.7	107.8 ± 1.8	98.1 ± 2.6	78.0 ± 1.7	72.5 ± 1.9	119.0 ± 2.8
micelle	$R_{tot,eq}$ (Å)	66.2 ± 0.4	78.5 ± 0.4	78.0 ± 0.2	73.8 ± 0.3	64.0 ± 0.2	59.0 ± 0.2	70.4 ± 0.3
	$R_{tot,pol}$ (Å)	416.8 ± 7.3	361.9 ± 5.9	338.1 ± 3.4	356.7 ± 5.2	268.0 ± 3.1	279.4 ± 3.7	379.1 ± 5.4
	Σ	0.35	0.31	0.31	0.31	0.25	0.31	0.36
	φ_i	0.138	0.180	0.212	0.262	0.260	0.239	0.138
	N_{agg}	312	491	404	414	269	208	355

Table 3. Equatorial distance between the outer shells of two micelles, $d_{micelle}$, of PLA-PEO-PLA systems with different L/D ratios at 10 wt%.

Sample	***d*-spacing (Å)**	$d_{micelle}$
S 50/50	356	224
S 75/25	350	193
S 80/20	345	189

S 85/15	314	166
S 90/10	253	125
S 95/5	241	123
S 100/0	323	182

To validate the micellar parameters obtained by fitting, the parameters can be quantitatively compared to the chain contour length L and end-to-end distance r_{ed}. Calculations of these parameters are described and given in the Supplementary Information (Table S2). In general, the equatorial thickness of PEO shell is comparable to the end-to-end distance of PEO block in a theta solvent, indicating that the PEO chains in the shell are coiled. By contrast, the radius of the core at the equator is closer to the contour length of PLA block, indicating the PLA chains are in a stretched conformation. This may be due to the formation of PLA crystals in the core. The mobility of the PLA block segments on both sides of PEO block in ABA architectures is lower compared to that of the PLA block in PLA-PEO diblock copolymers. The inhomogeneous PEO shell will thus interfere with the formation of a uniformly spherical hydrophobic domain to a greater degree for triblock copolymers, which possibly promotes the stretched arrangement of PLA blocks and the formation of ellipsoidal core with partially crystalline domains.

At a lower concentration of 2 wt%, the core-shell sphere, sphere, and core-shell ellipsoid model all did not provide satisfactory fitting profiles, particularly in the mid-q range. However, a simple ellipsoid model generated fits with good agreement (Table 4). The overall scattering intensity for the ellipsoid model with orientation [54] is given by:

$$\mathrm{I}(q) = \frac{\mathrm{scale}}{V}\mathrm{P}^2(q,\alpha) + \mathrm{background} \qquad (6)$$

where

$$\mathrm{P}(q,\alpha) = \Delta\rho V \frac{3(\sin q\mathrm{m} - q\mathrm{m}\cos q\mathrm{m})}{(q\mathrm{m})^3} \quad (7)$$

and

$$\mathrm{m} = \left(R_{equat}^2 \sin^2\alpha + R_{polar}^2 \cos^2\alpha\right)^{0.5} \quad (8)$$

The fitting results obtained further support the soundness of micellar parameters obtained for L/D systems at higher concentrations utilizing the core-shell ellipsoid model. The equatorial and polar radii of micelles with the simple ellipsoid model at 2 wt% are both comparable to those for systems at higher concentrations and follow the trends described above.

Table 4. Parameters of micelle in ellipsoid model of PLA-PEO-PLA systems with different L/D ratios at 2 wt%.

	L/D 50/50	L/D 75/25	L/D 80/20	L/D 85/15	L/D 90/10	L/D 95/5	L/D 100/0
R_{equat} (Å)	82.5 ± 0.1	84.6 ± 0.1	85.9 ± 0.1	82.9 ± 0.1	62.7 ± 0.1	59.9 ± 0.1	76.4 ± 0.1
R_{polar} (Å)	484.4 ± 2.6	380.7 ± 0.6	379.4 ± 0.5	361.3 ± 0.5	265.7 ± 0.6	279.9 ± 0.7	439.3 ± 1.5
Σ	0.31	0.35	0.29	0.32	0.32	0.33	0.35
φ_i	0.092	0.180	0.234	0.247	0.260	0.250	0.119

5. Conclusions

We present a SANS study of hydrogels and aqueous solutions of PLA-PEO-PLA block copolymers with L/D ratios of the PLA block varying from 50/50 to 100/0. The effect of PLA block stereochemistry on the nanoscale assembly of copolymer micelles is examined. Correlation peaks are observed for all the copolymers at higher concentrations. Lowering the concentration causes the transition from correlation peaks to shoulders for most of copolymers except for triblocks with L/D ratios of 85/15, 90/10, and 95/5. In addition, the peak position for these

samples does not vary with concentration. This suggests inhomogeneity in these gels, with local regions where strongly-associating micelles may be more closely-spaced. The high q features we observe via a Kratky plot suggest the use of an ellipsoidal form factor model for the micelles. The structural parameters obtained for different L/D systems from model fitting show high aggregation numbers for systems with L/D ratios of 75/25, 80/20, and 85/15, consistent with a strong interaction between PLA chains in these systems. A smaller overall micelle size and intermicellar distance was observed for the 90/10 and 95/5 systems. Both of these trends are consistent with our rheological data from previous studies, which showed a high storage modulus for samples at intermediate L/D ratios, which we hypothesized to be due to both a longer endblock pull-out time for PLA chains and a greater fraction of bridging chains. These findings provide insight into the use of stereochemistry as means of tuning both the nanoscale assembly and mechanical properties in amphiphilic block copolymers.

6. Acknowledgements

The authors gratefully acknowledge financial support from NSF awards CBET-1335787 and DMR-1905547; ACS PRF grant 55729-ND9; a Turner Dissertation Fellowship for D.R.O.H; and a Department of Education GAANN Fellowship (Award P200A160163) for S.P.Q. and B.Z. This research used resources at the Spallation Neutron Source, a DOE Office of Science User Facility operated by the Oak Ridge National Laboratory. This research work benefited from the use of the SasView application, originally developed under NSF award DMR-0520547. SasView contains code developed with funding from the European Union's Horizon 2020 research and innovation programme under the SINE2020 project, grant agreement No 654000.

References

(1) Gong, J. P.; Katsuyama, Y.; Kurokawa, T.; Osada, Y. Double-network hydrogels with extremely high mechanical strength. *Adv Mater* **2003**, *15*, 1155-+.

(2) Nair, L. S.; Laurencin, C. T. Biodegradable polymers as biomaterials. *Prog Polym Sci* **2007**, *32*, 762-798.

(3) Bae, Y.; Fukushima, S.; Harada, A.; Kataoka, K. Design of environment-sensitive supramolecular assemblies for intracellular drug delivery: Polymeric micelles that are responsive to intracellular pH change. *Angew Chem Int Edit* **2003**, *42*, 4640-4643.

(4) Agrawal, S. K.; Sanabria-DeLong, N.; Tew, G. N.; Bhatia, S. R. Structural characterization of PLA-PEO-PLA solutions and hydrogels: Crystalline vs amorphous PLA domains. *Macromolecules* **2008**, *41*, 1774-1784.

(5) Khorshid, N. K.; Zhu, K. Z.; Knudsen, K. D.; Bekhradnia, S.; Sande, S. A.; Nystrom, B. Novel Structural Changes during Temperature-Induced Self-Assembling and Gelation of PLGA-PEG-PLGA Triblock Copolymer in Aqueous Solutions. *Macromol Biosci* **2016**, *16*, 1838-1852.

(6) Mai, Y. Y.; Eisenberg, A. Self-assembly of block copolymers. *Chem Soc Rev* **2012**, *41*, 5969-5985.

(7) Zhang, Q.; Lin, J. P.; Wang, L. Q.; Xu, Z. W. Theoretical modeling and simulations of self-assembly of copolymers in solution. *Prog Polym Sci* **2017**, *75*, 1-30.

(8) Chen, Y. H.; Zhou, S. W.; Li, Q. Mathematical modeling of degradation for bulk-erosive polymers: Applications in tissue engineering scaffolds and drug delivery systems. *Acta Biomater* **2011**, *7*, 1140-1149.

(9) Zhang, H. B.; Zhou, L.; Zhang, W. J. Control of Scaffold Degradation in Tissue Engineering: A Review. *Tissue Eng Part B-Re* **2014**, *20*, 492-502.

(10) Shirazi, R. N.; Ronan, W.; Rochev, Y.; McHugh, P. Modelling the degradation and elastic properties of poly(lactic-co-glycolic acid) films and regular open -cell tissue engineering scaffolds. *J Mech Behav Biomed* **2016**, *54*, 48-59.

(11) Calo, E.; Khutoryanskiy, V. V. Biomedical applications of hydrogels: A review of patents and commercial products. *Eur Polym J* **2015**, *65*, 252-267.

(12) Laycock, B.; Nikolic, M.; Colwell, J. M.; Gauthier, E.; Halley, P.; Bottle, S.; George, G. Lifetime prediction of biodegradable polymers. *Prog Polym Sci* **2017**, *71*, 144-189.

(13) Farah, S.; Anderson, D. G.; Langer, R. Physical and mechanical properties of PLA, and their functions in widespread applications - A comprehensive review. *Adv Drug Deliver Rev* **2016**, *107*, 367-392.

(14) Duval, M.; Gross, E. Degradation of Poly(ethylene oxide) in Aqueous Solutions by Ultrasonic Waves. *Macromolecules* **2013**, *46*, 4972-4977.

(15) Aamer, K. A.; Sardinha, H.; Bhatia, S. R.; Tew, G. N. Rheological studies of PLLA-PEO-PLLA triblock copolymer hydrogels. *Biomaterials* **2004**, *25*, 1087-1093.

(16) Agrawal, S. K.; Sanabria-DeLong, N.; Bhatia, S. K.; Tew, G. N.; Bhatia, S. R. Energetics of Association in Poly(lactic acid)-based Hydrogels with Crystalline and Nanoparticle- Polymer Junctions. *Langmuir* **2010**, *26*, 17330-17338.

(17) Sanabria-DeLong, N.; Agrawal, S. K.; Bhatia, S. R.; Tew, G. N. Controlling hydrogel properties by crystallization of hydrophobic domains. *Macromolecules* **2006**, *39*, 1308-1310.

(18) Abebe, D. G.; Fujiwara, T. Controlled Thermoresponsive Hydrogels by

Stereocomplexed PLA-PEG-PLA Prepared via Hybrid Micelles of Pre-Mixed Copolymers with Different PEG Lengths. *Biomacromolecules* **2012**, *13*, 1828-1836.

(19) Posocco, P.; Fermeglia, M.; Pricl, S. Morphology prediction of block copolymers for drug delivery by mesoscale simulations. *J Mater Chem* **2010**, *20*, 7742-7753.

(20) Liao, M. R.; Liu, H. Y.; Guo, H. Y.; Zhou, J. Mesoscopic Structures of Poly(carboxybetaine) Block Copolymer and Poly(ethylene glycol) Block Copolymer in Solutions. *Langmuir* **2017**, *33*, 7575-7582.

(21) Sun, L.; Pitto-Barry, A.; Kirby, N.; Schiller, T. L.; Sanchez, A. M.; Dyson, M. A.; Sloan, J.; Wilson, N. R.; O'Reilly, R. K.; Dove, A. P. Structural reorganization of cylindrical nanoparticles triggered by polylactide stereocomplexation. *Nat Commun* **2014**, *5*.

(22) Yu, W.; Inam, M.; Jones, J. R.; Dove, A. P.; O'Reilly, R. K. Understanding the CDSA of poly(lactide) containing triblock copolymers. *Polym Chem-Uk* **2017**, *8*, 5504-5512.

(23) Inam, M.; Cambridge, G.; Pitto-Barry, A.; Laker, Z. P. L.; Wilson, N. R.; Mathers, R. T.; Dove, A. P.; O'Reilly, R. K. 1D vs. 2D shape selectivity in the crystallization-driven self-assembly of polylactide block copolymers. *Chem Sci* **2017**, *8*, 4223-4230.

(24) Cao, H. Q.; Chang, X. H.; Mao, H. L.; Zhou, J.; Wu, Z. L.; Shan, G. R.; Bao, Y. Z.; Pan, P. J. Stereocomplexed physical hydrogels with high strength and tunable crystallizability. *Soft Matter* **2017**, *13*, 8502-8510.

(25) Hsu, Y. I.; Masutani, K.; Yamaoka, T.; Kimura, Y. Tuning of Sol-Gel Transition in the Mixed Polymer Micelle Solutions of Copolymer Mixtures Consisting of Enantiomeric Diblock and Triblock Copolymers of Polylactide and Poly(ethylene glycol). *Macromol Chem Phys* **2015**, *216*, 837-846.

(26) Ikada, Y.; Jamshidi, K.; Tsuji, H.; Hyon, S. H. Stereocomplex Formation between Enantiomeric Poly(Lactides). *Macromolecules* **1987**, *20*, 904-906.

(27) Agrawal, S. K.; Sanabria-DeLong, N.; Tew, G. N.; Bhatia, S. R. Rheological characterization of biocompatible associative polymer hydrogels with crystalline and amorphous endblocks. *Journal of Materials Research* **2006**, *21*, 2118-2125.

(28) Agrawal, S. K.; Sanabria-DeLong, N.; Jemian, P. R.; Tew, G. N.; Bhatia, S. R. Micro- to nanoscale structure of biocompatible PLA-PEO-PLA hydrogels. *Langmuir* **2007**, *23*, 5039-5044.

(29) Agrawal, S. K.; Sanabria-DeLong, N.; Coburn, J. M.; Tew, G. N.; Bhatia, S. R. Novel drug release profiles from micellar solutions of PLA-PEO-PLA triblock copolymers. *J Control Release* **2006**, *112*, 64-71.

(30) Yin, X. C.; Hewitt, D. R. O.; Quah, S. P.; Zheng, B. Q.; Mattei, G. S.; Khalifah, P. G.; Grubbs, R. B.; Bhatia, S. R. Impact of stereochemistry on rheology and nanostructure of PLA-PEO-PLA triblocks: stiff gels at intermediate l/d-lactide ratios. *Soft Matter* **2018**, *14*, 7255-7263.

(31) Yin, X.; Hewitt, D. R. O.; Preston, A. N.; Heroux, L. A.; Agamalian, M. M.; Quah, S. P.; Zheng, B.; Smith, A. J.; Laughlin, S. T.; Grubbs, R. B.; Bhatia, S. R. Hierarchical assembly in PLA-PEO-PLA hydrogels with crystalline domains and effect of block stereochemistry. *Colloids Surf B Biointerfaces* **2019**, *180*, 102-109.

(32) Agarwal, R.; Alam, M. S.; Gupta, B. Preparation of Curcumin Loaded Poly(Vinyl Alcohol)-Poly(Ethylene Oxide)-Carboxymethyl Cellulose Membranes for Wound Care Application. *J Biomater Tiss Eng* **2013**, *3*, 273-283.

(33) Li, F.; Li, S. M.; Vert, M. Synthesis and rheological properties of polylactide/poly(ethylene glycol) multiblock copolymers. *Macromol Biosci* **2005**, *5*, 1125-1131.

(34) Brown, H. A.; De Crisci, A. G.; Hedrick, J. L.; Waymouth, R. M. Amidine-Mediated Zwitterionic Polymerization of Lactide. *Acs Macro Lett* **2012**, *1*, 1113-1115.

(35) Dove, A. P. Organic Catalysis for Ring-Opening Polymerization. *Acs Macro Lett* **2012**, *1*, 1409-1412.

(36) Arnold, O.; Bilheux, J. C.; Borreguero, J. M.; Buts, A.; Campbell, S. I.; Chapon, L.; Doucet, M.; Draper, N.; Ferraz Leal, R.; Gigg, M. A.; Lynch, V. E.; Markvardsen, A.; Mikkelson, D. J.; Mikkelson, R. L.; Miller, R.; Palmen, K.; Parker, P.; Passos, G.; Perring, T. G.; Peterson, P. F.; Ren, S.; Reuter, M. A.; Savici, A. T.; Taylor, J. W.; Taylor, R. J.; Tolchenov, R.; Zhou, W.; Zikovsky, J. Mantid—Data analysis and visualization package for neutron scattering and μ SR experiments. *Nuclear Instruments and Methods in Physics Research Section A: Accelerators, Spectrometers, Detectors and Associated Equipment* **2014**, *764*, 156-166.

(37) Wignall, G. D.; Bates, F. S. Absolute Calibration of Small-Angle Neutron-Scattering Data. *J Appl Crystallogr* **1987**, *20*, 28-40.

(38) Lebouille, J. G. J. L.; Leermakers, F. A. M.; Stuart, M. A. C.; Tuinier, R. Design of block-copolymer-based micelles for active and passive targeting. *Phys Rev E* **2016**, *94*.

(39) Lee, E. S.; Oh, K. T.; Kim, D.; Youn, Y. S.; Bae, Y. H. Tumor pH-responsive flower-like micelles of poly(L-lactic acid)-b-poly (ethylene glycol)-b-poly(L-histidine). *J Control Release* **2007**, *123*, 19-26.

(40) Honda, S.; Yamamoto, T.; Tezuka, Y. Tuneable enhancement of the salt and thermal stability of polymeric micelles by cyclized amphiphiles. *Nat Commun* **2013**, *4*.

(41) de Graaf, A. J.; Boere, K. W. M.; Kemmink, J.; Fokkink, R. G.; van Nostrum, C. F.; Rijkers, D. T. S.; van der Gucht, J.; Wienk, H.; Baldus, M.; Mastrobattista, E.; Vermonden, T.; Hennink, W. E. Looped Structure of Flowerlike Micelles Revealed by H-1 NMR Relaxometry and Light Scattering. *Langmuir* **2011**, *27*, 9843-9848.

(42) Fuertes, G.; Banterlea, N.; Ruff, K. M.; Chowdhury, A.; Mercadante, D.; Koehler, C.; Kachala, M.; Girona, G. E.; Milles, S.; Mishra, A.; Onck, P. R.; Grater, F.; Esteban-Martin, S.; Pappu, R. V.; Svergun, D. I.; Lemke, E. A. Decoupling of size and shape fluctuations in heteropolymeric sequences reconciles discrepancies in SAXS vs. FRET measurements. *P Natl Acad Sci USA* **2017**, *114*, E6342-E6351.

(43) Hadziioannou, G.; Cotts, P. M.; Tenbrinke, G.; Han, C. C.; Lutz, P.; Strazielle, C.; Rempp, P.; Kovacs, A. J. Thermodynamic and Hydrodynamic Properties of Dilute-Solutions of Cyclic and Linear Polystyrenes. *Macromolecules* **1987**, *20*, 493-497.

(44) Etampawala, T. N.; Aryal, D.; Osti, N. C.; He, L. L.; Heller, W. T.; Willis, C. L.; Grest, G. S.; Perahia, D. Association of a multifunctional ionic block copolymer in a selective solvent. *J Chem Phys* **2016**, *145*.

(45) Kotlarchyk, M.; Chen, S. H. Analysis of Small-Angle Neutron-Scattering Spectra from Polydisperse Interacting Colloids. *J Chem Phys* **1983**, *79*, 2461-2469.

(46) Berr, S. S. Solvent Isotope Effects on Alkyltrimethylammonium Bromide Micelles as a Function of Alkyl Chain-Length. *J Phys Chem-Us* **1987**, *91*, 4760-4765.

(47) Seidel, C. Physics of amphiphiles: Micelles, vesicles and microemulsions. Proceedings of the International School of Physics “Enrico Fermi”, Cours XC at Varenna on Lake Como, 19–29 July 1983. Hg. von V. DEGIORGIO und M. CORTI. ISBN 0-444-86940-9. Amsterdam/Oxford/New York/Tokyo: North Holland Physics Publishing 1985. XXIV, 888 S., Lwd., Dfl. 400.00. Available in USA and Canada from Elsevier Science Publishers, 52 Vanderbilt Ave., New York, NY 10017, USA. *Acta Polymerica* **1986**, *37*, 474-474.

(48) Kinning, D. J.; Thomas, E. L. Hard-Sphere Interactions between Spherical

Domains in Diblock Copolymers. *Macromolecules* **1984**, *17*, 1712-1718.

(49) Foffi, G.; Savin, G.; Bucciarelli, S.; Dorsaz, N.; Thurston, G. M.; Stradner, A.; Schurtenberger, P. Hard sphere-like glass transition in eye lens alpha-crystallin solutions. *P Natl Acad Sci USA* **2014**, *111*, 16748-16753.

(50) Pedersen, J. S.; Svaneborg, C. Scattering from block copolymer micelles. *Curr Opin Colloid In* **2002**, *7*, 158-166.

(51) Peters, A. J.; Lodge, T. P. Chain Exchange Kinetics of Asymmetric B(1)AB(2) Linear Triblock and AB(1)B(2) Branched Triblock Copolymers. *Macromolecules* **2017**, *50*, 6303-6313.

(52) Seitz, M. E.; Rottsolk, R. L.; Shull, K. R. Effect of Homopolymer Solubilization on Triblock Gel Structure and Mechanical Response. *J Polym Sci Pol Phys* **2010**, *48*, 1395-1408.

(53) Sliozberg, Y. R.; Strawhecker, K. E.; Andzelm, J. W.; Lenhart, J. L. Computational and experimental investigation of morphology in thermoplastic elastomer gels composed of AB/ABA blends in B-selective solvent. *Soft Matter* **2011**, *7*, 7539-7551.

(54) Svergun, D. I.; Feĭgin, L. A.; Taylor, G. W.: *Structure analysis by small-angle x-ray and neutron scattering*; Plenum Press: New York, 1987.